

## Noninvasive electrical detection of electron spin dynamics at the N atom in N@C<sub>60</sub>

This article has been downloaded from IOPscience. Please scroll down to see the full text article.

2010 J. Phys.: Condens. Matter 22 295305

(<http://iopscience.iop.org/0953-8984/22/29/295305>)

View [the table of contents for this issue](#), or go to the [journal homepage](#) for more

Download details:

IP Address: 128.18.31.192

The article was downloaded on 16/08/2010 at 20:12

Please note that [terms and conditions apply](#).

# Noninvasive electrical detection of electron spin dynamics at the N atom in N@C<sub>60</sub>

Z G Yu

Physical Sciences Division, SRI International, 333 Ravenswood Avenue, Menlo Park, CA 94025, USA

E-mail: [zhi-gang.yu@sri.com](mailto:zhi-gang.yu@sri.com)

Received 7 April 2010, in final form 26 May 2010

Published 2 July 2010

Online at [stacks.iop.org/JPhysCM/22/295305](http://stacks.iop.org/JPhysCM/22/295305)

## Abstract

Endohedral N@C<sub>60</sub> contains an electron spin of  $S = 3/2$  at the central N atom, which, shielded by the C<sub>60</sub> cage, has an extremely long spin relaxation time. The  $\pi$ -conjugated C<sub>60</sub> cage, when connected to electrodes, provides a highly conductive path for electron transport and enables a noninvasive electrical detection of dynamics of the central spin. Here we use the Keldysh non-equilibrium Green's function and establish a microscopic description of how spin dynamics, including resonance and relaxation, can manifest itself in the device conductance. We predict that magnetic electrodes can enhance the detectivity by orders of magnitude compared with nonmagnetic electrodes. It is shown that this electrical detection is more sensitive to the longitudinal spin component than the transverse one. Hence the transient spin nutation is particularly useful in determining spin decoherence time  $T_2$  in such transport device structures. This theory can be used to describe recent experiments of electrically detected spin dynamics in C<sub>60</sub> and other systems.

(Some figures in this article are in colour only in the electronic version)

## 1. Introduction

The electron spin at the central N atom in endohedral N@C<sub>60</sub> exhibits an extraordinarily long electron spin relaxation time [1] and can be manipulated by a variety of microwave pulse sequences [2], showing its great potential in quantum information storage and processing [3]. The long relaxation time was ascribed to the high-order two-phonon Raman process [1, 4]. For applications in the fields of quantum information and spintronics, it is desired that dynamics of individual spins rather than an ensemble average of spins be measured and recorded [5], which requires a highly sensitive probe of electron spin resonance (ESR) and, more generally, spin dynamics. ESR, which is commonly measured from microwave absorption, can also be detected electrically by observing the change in the conductivity of the system [6] and electrically detected ESR (EDES) has been extensively used in studies of defects in semiconductors with sensitivity often higher than conventional ESR detection by several orders of magnitude [6]. In N@C<sub>60</sub>, because of the intimate coupling ( $10^{-4}$ – $10^{-3}$  eV [7, 8]) between the central spin and delocalized  $\pi$  electrons in the conjugated C<sub>60</sub>, as well as the high conductance (1–100 nS [9]) of a C<sub>60</sub> molecule, we

expect that a much higher sensitivity in EDES, possibly to a single molecule resolution, can be achieved. This electrical detection of spin dynamics is noninvasive in that an injected electron into N@C<sub>60</sub> would traverse along the  $\pi$ -conjugated pathways without spoiling the central spin at the N atom. This is in contrast to quantum dots and related structures where an injected electron into a system with an electron spin would destroy the original spin (invasive), resulting in the loss of quantum information contained in that spin [10].

In this paper, using the Keldysh non-equilibrium Green's functions, we express that conductance in terms of the Green's function of N@C<sub>60</sub>, which depends on the central spin in a straightforward manner. The Keldysh Green's function provides a systematic way to retain quantum coherence (phase information) in electrical transport, an essential component in detecting spin dynamics. Moreover, it allows easy incorporation of many-body effects by renormalizing the Green's function of N@C<sub>60</sub> without altering the relation between the transport signal and the Green's function. With the combination of static and microwave magnetic fields, the spin dynamics can be manipulated, which can effect change in the device conductance. We predict that ferromagnetic electrodes can enhance the conductance change by orders of magnitude

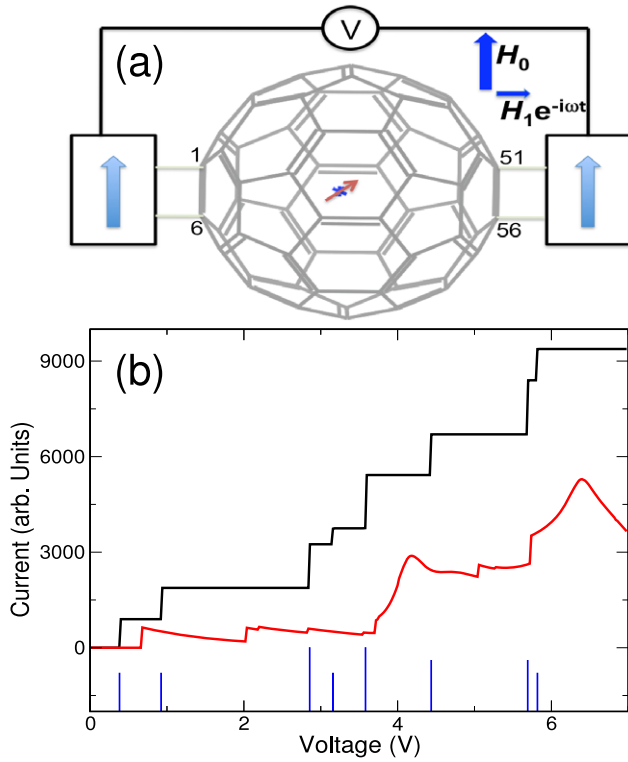


**Figure 1.** (a) Schematic diagram of electrical detection of electron spin dynamics in the ferromagnet/N@C<sub>60</sub>/ferromagnetic structure. The central N atom inside the C<sub>60</sub> cage has an electron spin  $S = 3/2$ . Electrons flow in C<sub>60</sub> from the magnetic electrodes via the four C atoms (1, 6, 51 and 56). The static and microwave magnetic fields,  $H_0$  and  $H_1$ , are used to change spin dynamics. An electrical gate (not shown) can be included to modify the charge state of N@C<sub>60</sub>. (b)  $I$ - $V$  characteristics of the device structure in equilibrium ( $H_1 = 0$ ). The black line describes the case where the site energy in a neutral C<sub>60</sub> is independent of voltage and the red (gray) line describes the case where the site energy change is proportional to the voltage. The blue bars indicate the energy levels of a neutral C<sub>60</sub> and the bar height represents the energy degeneracy.

compared with nonmagnetic ones. This electrical detection of spin dynamics, as shown later in this paper, is much more sensitive to the longitudinal spin component than the transverse one, suggesting that a higher sensitivity may be achieved if one can associate the property to be measured with the longitudinal component via, for example, the transient nutation [11], where the longitudinal component is precessing around the  $x$  axis in the rotating frame. Previous theoretical and experimental studies of electrical transport across N@C<sub>60</sub> focus on the effect of different charged states in the C<sub>60</sub> on transport in the sequential tunneling regime [7, 8]. In this paper, however, we are primarily concerned with a non-resonant, low-voltage transport process (co-tunneling regime) that allows a quick response in electrical transport to the spin dynamics. The present work is also motivated by recent experiments that demonstrate pulsed EDESr is capable of detecting coherent spin dynamics in C<sub>60</sub> [12] and  $\pi$ -conjugated-polymer [13] device structures. Our microscopic theory can reproduce many features observed in those systems, suggesting its versatility and usefulness in describing EDESr experiments in a variety of nanostructures.

This paper is organized as follows. First, we derive in section 2 a Keldysh non-equilibrium Green's function formalism that connects the electrical current and the spin-polarized Green's functions of N@C<sub>60</sub>. In section 3, we evaluate the Green's functions of N@C<sub>60</sub> and express them as a function of the central spin at the N atom. Then, in section 4, we study dynamics of the central spin and its effects on electrical current using the Bloch equations and the obtained Green's function formalism. Finally, we summarize our results in section 5.

## 2. Keldysh non-equilibrium Green's function formalism

We consider a device structure (shown in figure 1), where an N@C<sub>60</sub> molecule is placed between two metallic electrodes. A scanning tunneling microscope (STM) tip can also serve as an electrode [14]. A DC magnetic field  $H_0$  is along the  $z$  axis,  $H_0 = H_0 e_z$ , and the microwave magnetic  $H_1$  is in the  $x$ - $y$  plane. To make our results specific and verifiable, we assume in our calculations that the bonds between C(1) and C(6) and between C(51) and C(56) are parallel to the electrodes, and these four C atoms have the shortest distance to the electrodes. However, our results, which will be expressed as a change in conductance between situations in the presence and in the absence of spin dynamics, are not sensitive to the relative geometry between the C<sub>60</sub> and the electrodes. The proposed device structure is experimentally feasible since all essential components have been successfully demonstrated: Electrical conduction through a single N@C<sub>60</sub> between metal electrodes has been measured [8] and both steady-state and pulsed EDESr has been performed in related  $\pi$ -conjugated systems including C<sub>60</sub> [12] and conductive polymers [13].

When a C<sub>60</sub> molecule is attached to an electrode, depending on their relative work functions, the C<sub>60</sub> can remain neutral or become charged. If the C<sub>60</sub> has an odd number of excess charges ( $\pm 1, 3$ , etc), the unpaired electron will give rise to an electron spin, which would interfere with the dynamics of the spin at the central N atom. Hence for an unambiguous detection of spin dynamics on the N atom, we will confine us to the N@C<sub>60</sub> with zero or an even number of excess charge (which can be achieved by choosing a proper electrode [14] or using an electrical gate [8]), where the electron spin is solely from the central N atom because the ground state in neutral and charged C<sub>60</sub> usually is a spin singlet rather than a triplet.

The Hamiltonian of the system comprises four parts:

$$H = H_\alpha + H_{\alpha'} + H_{N@C_{60}} + H_C. \quad (1)$$

Here  $H_{\alpha(\alpha')}$  describes the left (right) electrode, which is assumed to be a conventional metal or ferromagnet, with a Fermi energy  $\mu_{\alpha(\alpha')}$  and a spin-polarized density of states,  $\rho_{\alpha(\alpha')}(\omega) = \rho_{\alpha(\alpha')\uparrow}(\omega) + \rho_{\alpha(\alpha')\downarrow}(\omega)$ , where  $\omega$  is the energy.  $H_{N@C_{60}}$  represents an isolated endohedral N@C<sub>60</sub> molecule,  $H_{N@C_{60}} = H_{C_{60}} + H_{ex}$ , where  $H_{C_{60}}$  is the Hamiltonian of a C<sub>60</sub> molecule:

$$H_{C_{60}} = - \sum_{(ij)\sigma} [t_0 - \alpha_0(d_{ij} - d_0)](c_{i\sigma}^\dagger c_{j\sigma} + \text{H.c.}) + \sum_{i\sigma} \epsilon_i(V) c_{i\sigma}^\dagger c_{i\sigma} + \frac{1}{2} K \sum_{(ij)} (d_{ij} - d_0)^2. \quad (2)$$

and  $H_{\text{ex}}$  is the exchange interaction between electrons in  $C_{60}$  and the central spin  $S$  at the N atom:

$$H_{\text{ex}} = J \sum_{i\sigma\sigma'} c_{i\sigma}^\dagger \hat{\sigma}_{\sigma\sigma'} c_{i\sigma'} \cdot S. \quad (3)$$

Here we use a tight-binding  $\pi$ -electron model for  $C_{60}$ , which resembles the Su–Schrieffer–Heeger (SSH) model for  $\pi$ -conjugated polymers [17].  $c_{i\sigma}^\dagger$  creates a  $\pi$  electron at site  $i$  with spin  $\sigma$  ( $\uparrow$  or  $\downarrow$ ) along the spin quantization axis  $e_z$ , i.e. the direction of  $H_0$ ,  $\alpha_0$  is the electron–lattice coupling,  $d_{ij}$  is the bond length between the adjacent  $i$ th and  $j$ th atoms, and  $K$  is the elastic constant for C–C  $\sigma$  bonds.  $\epsilon_i$  is the electron energy at site  $i$ , which is a function of an applied voltage  $V$ . This SSH-like Hamiltonian is proven to be reliable in predicting  $C_{60}$  electronic and bond structures [18]. The coupling between the spin at the central N atom,  $S$ , and  $\pi$  electrons in the  $C_{60}$  cage is through an exchange interaction, which originates from the overlap between electron wavefunctions of the N atom and of the  $C_{60}$ , and  $\hat{\sigma}$  are Pauli matrices. The exchange strength, according to both theory and experiment [7, 8], is about  $J = 10^{-4}$  eV.  $H_C$  is the coupling between the electrodes and N@ $C_{60}$ , and it is assumed that only the four atoms that are closest to the electrodes have a direct electronic coupling to the electrodes:

$$H_C = \sum_{\sigma\sigma', a=\{1,5\}} [T_{\sigma\sigma'} c_{a\sigma}^\dagger c_{a\sigma'} + T_{\sigma'\sigma}^* c_{a\sigma'}^\dagger c_{a\sigma}] + \sum_{\sigma\sigma', b=\{51,56\}} [T'_{\sigma\sigma'} c_{b\sigma}^\dagger c_{b\sigma'} + T'^*_{\sigma'\sigma} c_{b\sigma'}^\dagger c_{b\sigma}], \quad (4)$$

where  $c_{a\sigma}^\dagger$  ( $c_{a'\sigma}^\dagger$ ) creates an electron with spin  $\sigma$  in the left (right) electrode along the electrode magnetization,  $\mathbf{m}_{L(R)}$ , and  $T_{\sigma\sigma'}$  ( $T'_{\sigma\sigma'}$ ) is the electron hopping matrix element from spin  $\sigma$  in the  $C_{60}$  to the spin  $\sigma'$  in the left (right) electrode, which depends on the relative orientation between  $e_z$  and  $\mathbf{m}_{L(R)}$ . One possible model for  $T$  and  $T'$  is that the spin dependence is due purely to an  $SU(2)$  spin rotation:

$$T = t \begin{pmatrix} \cos \frac{\theta_L}{2} e^{i\phi_L/2} & \sin \frac{\theta_L}{2} e^{i\phi_L/2} \\ -\sin \frac{\theta_L}{2} e^{-i\phi_L/2} & \cos \frac{\theta_L}{2} e^{-i\phi_L/2} \end{pmatrix}, \\ T' = t' \begin{pmatrix} \cos \frac{\theta_R}{2} e^{i\phi_R/2} & \sin \frac{\theta_R}{2} e^{i\phi_R/2} \\ -\sin \frac{\theta_R}{2} e^{-i\phi_R/2} & \cos \frac{\theta_R}{2} e^{-i\phi_R/2} \end{pmatrix},$$

where  $\mathbf{m}_{L(R)} = (\sin \theta_{L(R)} \cos \phi_{L(R)}, \sin \theta_{L(R)} \sin \phi_{L(R)}, \cos \theta_{L(R)})^T$ ,  $t$  and  $t'$  are the magnitudes of the hopping integral. These hopping matrices exclude spin-flip hopping between the electrode and the molecule. When the spin-flip hopping is not entirely forbidden, due, for example, to the spin–orbit coupling in the electrode,  $T_{\sigma\sigma'}$  ( $T'_{\sigma\sigma'}$ ) should be augmented by  $\delta T_{\sigma\sigma'}$  ( $\delta T'_{\sigma\sigma'}$ ):

$$\delta T = t \begin{pmatrix} -\lambda^* \sin \frac{\theta_L}{2} e^{i\phi_L/2} & \lambda \cos \frac{\theta_L}{2} e^{-i\phi_L/2} \\ \lambda^* \cos \frac{\theta_L}{2} e^{i\phi_L/2} & \lambda \sin \frac{\theta_L}{2} e^{-i\phi_L/2} \end{pmatrix}, \\ \delta T' = t' \begin{pmatrix} -\lambda^* \sin \frac{\theta_R}{2} e^{i\phi_R/2} & \lambda \cos \frac{\theta_R}{2} e^{-i\phi_R/2} \\ \lambda^* \cos \frac{\theta_R}{2} e^{i\phi_R/2} & \lambda \sin \frac{\theta_R}{2} e^{-i\phi_R/2} \end{pmatrix},$$

where  $\lambda \equiv \lambda_1 + i\lambda_2$  characterizes the relative importance of spin-flip hopping with respect to spin-conserved hopping and  $|\lambda|$  in general is much less than 1.

In the detection of coherent spin dynamics, it is important to retain the phase information. To this end, we use the Keldysh non-equilibrium Green's functions to evaluate the current across the electrode/N@ $C_{60}$ /electrode configuration. The current flowing out the left electrode is [15, 16]

$$I_L = -e \langle \dot{N}_L \rangle = \frac{-ie}{\hbar} \langle [H, N_L] \rangle \\ = \frac{e}{\hbar} \sum_{\sigma\sigma'} \int_{-\infty}^{+\infty} \frac{d\omega}{2\pi} [T_{\sigma\sigma'} G_{a\sigma, a\sigma'}^+(\omega) - T_{\sigma'\sigma}^* G_{a\sigma', a\sigma}^+(\omega)] \quad (5)$$

where  $N_L = \sum_{\alpha\sigma} c_{\alpha\sigma}^\dagger c_{\alpha\sigma}$ . The Green's functions  $G^+$  in the time domain are defined as  $G_{ij}^+(t, t') \equiv i \langle c_j^\dagger(t') c_i(t) \rangle$  and  $G_{ij}^-(t, t') \equiv -i \langle c_i(t) c_j^\dagger(t') \rangle$ . Using the Dyson equations for the non-equilibrium Green's functions [15]

$$G_{a\sigma', a\sigma}^+ - G_{a\sigma, a\sigma'}^+ = G_{a\sigma, a\tau}^- T_{\tau\tau'} g_{a\tau', a\sigma'}^+ - G_{a\sigma, a\tau}^+ T_{\tau\tau'} g_{a\tau', a\sigma'}^-$$

and

$$G_{a\sigma, a\sigma'}^\pm = G_{a\sigma, a\tau}^r T_{\tau\nu} g_{a\nu, a\sigma'}^\pm T_{\xi\xi}^* G_{a\xi, a\sigma'}^a,$$

with the advanced and retarded Green's functions in the time domain defined as  $G_{ij}^a(t, t') \equiv i\theta(t' - t) \langle \{c_i(t), c_j^\dagger(t')\} \rangle$  and  $G_{ij}^r(t, t') \equiv -i\theta(t - t') \langle \{c_i(t), c_j^\dagger(t')\} \rangle$ , where  $\theta(x)$  is the Heaviside step function and  $\{, \}$  is the anticommutator, as well as the electrode's Green's function in the frequency domain:

$$g_{\alpha\sigma, \alpha\sigma'}^+(\omega) = 2i\pi\theta(\mu_\alpha - \omega) \rho_{\alpha\sigma}(\omega) \delta_{\sigma\sigma'}, \\ g_{\alpha\sigma, \alpha\sigma'}^-(\omega) = -2i\pi\theta(\omega - \mu_\alpha) \rho_{\alpha\sigma}(\omega) \delta_{\sigma\sigma'},$$

we obtain that, for a device under an applied voltage  $V = (\mu_{\alpha'} - \mu_\alpha)/e$ :

$$I_L = \int_{\mu_L}^{\mu_L + eV} \frac{d\omega}{2\pi} g(\omega, V) \equiv \int_{\mu_L}^{\mu_L + eV} \frac{d\omega}{2\pi} \\ \times \sum_{a=\{1,6\}, b=\{51,56\}} \sum_{\eta\eta'} \frac{e}{\hbar} C_{\eta\eta'} A_{\eta'\eta} \quad (6)$$

where  $g(\omega, V)$  is the conductance and

$$C_{\eta\eta'} = T_{\eta\uparrow} \rho_{\alpha\uparrow}(\omega) T_{\uparrow\eta'} + T_{\eta\downarrow} \rho_{\alpha\downarrow}(\omega) T_{\downarrow\eta'}, \\ A_{\eta'\eta} = \sum_{\sigma\sigma'} G_{a\eta', b\sigma}^r(\omega) [T'_{\sigma\uparrow} \rho_{\alpha'\uparrow}(\omega) T'_{\uparrow\sigma'} \\ + T'_{\sigma\downarrow} \rho_{\alpha'\downarrow}(\omega) T'_{\downarrow\sigma'}] G_{b\sigma', a\eta}^a(\omega).$$

Equation (6) expresses the device conductance in terms of the Green's function of N@ $C_{60}$ ,  $G_{a\sigma, b\sigma'}^{r(a)}$ . Note that the Green's function  $G_{a\sigma, b\sigma'}^{r(a)}$  is the full Green's function with the effect of the electrodes contained in its self-energy. Consequently, as we will show in the next section, both sequential tunneling and co-tunneling processes are included in equation (6).

### 3. Green's functions of N@ $C_{60}$

In this section we evaluate the Green's function of the N@ $C_{60}$  molecule,  $G_{a\sigma, b\sigma'}^{r(a)}$ , and identify their dependence on the central spin  $S$ . Since the exchange energy between the central spin and  $C_{60}$  electrons,  $J = 10^{-4}$  eV, is very small compared to any energy scales in  $H_{C_{60}}$ , it does not affect the geometry of the

$C_{60}$ , which can be obtained by minimizing the total energy  $E_t$  (summation of  $\pi$ -electron energies and elastic energy from  $\sigma$  bonds) of the single-electron Hamiltonian  $H_{C_{60}}$ ,  $\partial E_t / \partial d_{ij} = 0$ . For the neutral  $C_{60}$ , the molecule has an  $I_h$  symmetry with the threefold-degenerate lowest unoccupied molecular orbital (LUMO) and the fivefold-degenerate highest occupied molecular orbital (HOMO) separated by 1.78 eV. For  $C_{60}^{2-}$  the excess charge causes a Jahn–Teller distortion, which reduces the symmetry from  $I_h$  to  $D_{5d}$  and removes the degeneracy of the electronic levels. The LUMO–HOMO gap is 0.02 eV from our calculation.

With the optimized geometry  $H_{N@C_{60}}$  can be written as

$$H_{N@C_{60}} = \sum_{m\sigma} \epsilon_m c_{m\sigma}^\dagger c_{m\sigma} + \sum_{m\sigma\sigma'} J_m c_{m\sigma}^\dagger \hat{\sigma}_{\sigma\sigma'} c_{m\sigma'}. \quad (7)$$

where  $\epsilon_m$  is the eigenenergy of the  $m$ th eigenstate,  $\psi_m$ ,  $c_m^\dagger$  creates an electron at the  $m$ th eigenstate and  $J_m = \sum_i \langle i | \psi_m \rangle \langle \psi_m | i \rangle = J$  is the exchange coupling between the  $m$ th eigenstate and  $S$ . To proceed further, we regard the N spin  $S$  as a magnetic impurity centered in the  $C_{60}$  cage and keep only the leading term of  $J$ , which is equivalent to treat  $S$  as a classical variable. Then the eigenenergy of each level is

$$\lambda_{m\pm} = \epsilon_m \pm J_m |\langle \hat{S} \rangle| \equiv \epsilon_m \pm J_m S, \quad (8)$$

where  $S = \sqrt{S_x^2 + S_y^2 + S_z^2}$  with  $S_q = \langle \hat{S}_q \rangle$  ( $q = x, y, z$ ), and  $\pm$  represents the up- and down-spin state along the direction of the averaged  $\langle \hat{S} \rangle$ . This semiclassical approximation, which neglects the Kondo effect, becomes inadequate in the resonant tunneling regime, where the incoming electron spends a considerable time in  $C_{60}$  and forms a bound state with  $S$ , but is reasonable in the non-resonant transport region, our main focus in this paper.

We see from equation (8) that the electron spin at the N atom acts as an effective magnetic field and gives rise to a Zeeman splitting between up and down spins for electrons in  $C_{60}$ . The Green's function in the spin space is a  $2 \times 2$  matrix, which can be written as a summation of a scalar and a vector:

$$\hat{G}_{ij}(\omega) = \begin{pmatrix} G_{i\uparrow j\uparrow} & G_{i\uparrow j\downarrow} \\ G_{i\downarrow j\uparrow} & G_{i\downarrow j\downarrow} \end{pmatrix} \equiv \bar{G}_{ij}^{r(a)}(\omega) \hat{1} + \mathbf{G}_{ij}^{r(a)}(\omega) \cdot \hat{\boldsymbol{\sigma}}. \quad (9)$$

We solve the Green's function from the definition  $(\omega + i\Gamma/2 - H_{N@C_{60}}) \hat{G}^r(\omega) = \hat{1}$  with  $\Gamma$  representing the broadening caused by other interactions not included in  $H_{N@C_{60}}$ , i.e. the coupling with the electrodes. The broadening due to the  $N@C_{60}$  electron excursion into the left electrode is the imaginary part of the self-energy,  $\text{Im}(t^2 g_{\alpha\alpha}^r) = t^2 \rho_\alpha(\omega)$ . If the broadening is much smaller than the exchange coupling  $J$ , we can use a spin-averaged broadening  $\Gamma$ , which can be estimated as

$$\Gamma(\omega) = \Gamma^L(\omega) + \Gamma^R(\omega) \simeq \frac{1}{2} [t^2 \rho_\alpha(\omega) + t'^2 \rho_{\alpha'}(\omega)],$$

where  $\Gamma^{L(R)}$  describes the contribution from the left (right) electrode:

$$\bar{G}_{ij}^r(\omega) = \sum_m \frac{(\omega - \epsilon_m) \langle i | \psi_m \rangle \langle \psi_m | j \rangle}{(\omega - \lambda_{m+} + i\Gamma/2)(\omega - \lambda_{m-} + i\Gamma/2)},$$

$$\mathbf{G}_{ij}^r(\omega) = \sum_m \frac{J_m \mathbf{S} \langle i | \psi_m \rangle \langle \psi_m | j \rangle}{(\omega - \lambda_{m+} + i\Gamma/2)(\omega - \lambda_{m-} + i\Gamma/2)} \equiv g_{ij}^r \mathbf{S}.$$

$\hat{G}_{ij}^a$  can be obtained by replacing  $\Gamma$  by  $-\Gamma$  in  $\hat{G}_{ij}^r$ . We see that the Green's function between any two sites in the  $C_{60}$  molecule depends on the central spin  $S$  in a transparent manner. To describe recent pulsed EDESR experiments in  $C_{60}$  and conjugated polymers [12, 13], a Hamiltonian as in equation (7) can be derived, with  $S$  being replaced by the average spin of the carriers (mean-field approximation) and the spin-polarized Green's functions in those systems have a similar form as in equation (9).

From the above Green's functions, we see that, when the energy of an incoming electron is far away from those of energy levels in  $N@C_{60}$ , i.e.  $\omega - \lambda_{m\pm} \gg \Gamma/2$ , the electrical current, according to equation (6), is proportional to  $t^2 t'^2$ , which describes the non-resonant co-tunneling process. The sequential tunneling process, which is proportional to  $t^2$  or  $t'^2$ , occurs when  $\omega - \lambda_{m+} \leq \Gamma/2$ . This becomes clear if we write equation (9) approximately as

$$I_L \propto \int d\omega \Gamma^L(\omega) \Gamma^R(\omega) \sum_{m\pm} \frac{1}{(\omega - \lambda_{m\pm})^2 + (\Gamma/2)^2},$$

which, if we approximate the Lorentzian function with the  $\delta$  function, becomes

$$\int d\omega \frac{\Gamma^L(\omega) \Gamma^R(\omega)}{\Gamma} \sum_{m\pm} \delta(\omega - \lambda_{m\pm}) \simeq \sum_{m\pm} \frac{\Gamma^L(\lambda_{m\pm}) \Gamma^R(\lambda_{m\pm})}{\Gamma},$$

and describes a sequential electron tunneling from the left electrode into an eigenstate of  $N@C_{60}$  and then out of the right electrode. Thus the Green's function formalism in equation (6) is sufficiently general and contains both the co-tunneling and sequential tunneling processes. The above expression also indicates that the sequential tunneling process is a resonant tunneling process, where the scattered electron is injected into and extracted from the eigenstates of  $N@C_{60}$ . The resonant process usually has a slow electrical response and therefore is not desired for the detection of fast spin dynamics. All numerical results presented in this paper are calculated by using the general expression of equation (6) and the Green's function of equation (9).

Before we examine the detection of spin dynamics, we calculate the overall  $I$ – $V$  characteristic of the ferromagnet/ $N@C_{60}$ /ferromagnet structure from our Green's function formalism in the absence of microwaves. This calculation can also help us identify the co-tunneling and sequential tunneling regions. As we mentioned earlier, because of the approximation we used, the results may become inaccurate in the resonant regions. Figure 1 displays the results for a neutral  $C_{60}$ , where  $\mu_\alpha$  was set equal to the site energy  $\epsilon_0$  at  $V = 0$  (in reality  $\mu_\alpha$ , depending on the material, may slightly deviate from  $\epsilon_0$ ). To see the connection between the electrical current and energy levels of  $C_{60}$ , we first assume the voltage dependence of the site energy,  $\epsilon_i \equiv \epsilon_0$ , a highly ideal case. As shown by the black line in figure 2(b), the current has abrupt jumps as the voltage increases, which coincides with the eigenenergies of  $C_{60}$ , indicating the resonant tunneling through these states. The first jump occurs around 0.4 V, i.e. at the energy of the

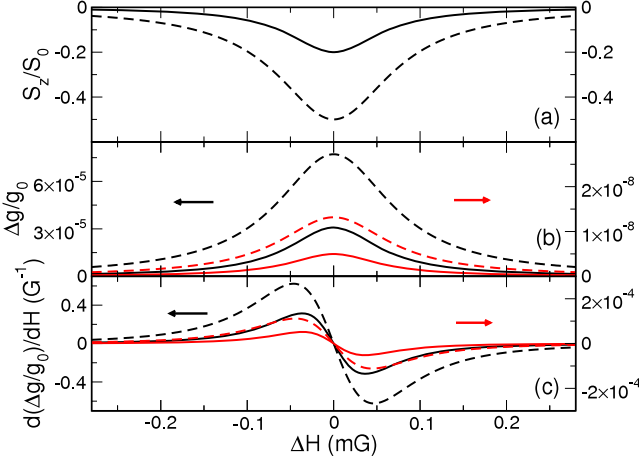


**Figure 2.** Electrically detected electron spin resonance in N@C<sub>60</sub> when slowly sweeping the DC magnetic field  $\mathbf{H}_0 = H_0 \mathbf{e}_z$  under a fixed microwave frequency  $\omega$ . Panels (a), (b) and (c) describe the longitudinal spin component  $S_z$ , relative conductance change  $\Delta g/g_0$  and derivative  $d(\Delta g/g_0)/dH_0$  as a function of  $\Delta H = H_0 - \omega/\gamma$ . Solid and dashed lines correspond to  $H_1 = 1/2\gamma\sqrt{T_1T_2}$  and  $1/\gamma\sqrt{T_1T_2}$ , respectively. Black (red or gray) lines are for ferromagnetic electrodes  $p_\alpha = p_{\alpha'} = 0.5$  (nonmagnetic electrodes  $p_\alpha = p_{\alpha'} = 10^{-4}$ ). The parameters are  $T_1 = 2T_2 = 2$  ms,  $\gamma = 1.76 \times 10^7 \text{ s}^{-1} \text{ G}^{-1}$ ,  $\omega = 5.28 \times 10^{10} \text{ s}^{-1}$ ,  $S_0 = 0.25$ ,  $\Gamma = 2 \times 10^{-5} \text{ eV}$  and  $J = 10^{-4} \text{ eV}$ .

LUMO ( $T_{1u}$ ) of a neutral C<sub>60</sub>. For a more realistic case, where  $\epsilon_i(V) = \epsilon_0 + (z/L)V$  with  $L$  being the distance between the two electrodes and  $z$  the distance between the  $i$ th C atom to the left electrode, the current also shows jumps but the locations for the jumps deviate from the eigenenergies of C<sub>60</sub>, as described by the red (gray) curve in figure 2(b). Similar results can also be obtained for C<sub>60</sub><sup>2-</sup> and the major difference is that the first jump in current occurs at much lower voltage ( $\sim 20$  mV) because the HOMO–LUMO gap in C<sub>60</sub><sup>2-</sup> from our calculation is 0.02 eV.

For detection of spin dynamics, a quick electrical response to spin dynamics is necessary. Thus we focus our attention in this paper on the non-resonant co-tunneling regime at a low voltage, where the current is controlled by conductance  $g(\mu_\alpha = \mu_{\alpha'} = \mu, V = 0)$ . At the Fermi level, the density of states for the electrodes can be approximately written as  $\rho_{\alpha\uparrow(\downarrow)}(\mu) = \rho_\alpha(\mu)[1 + (-)p_\alpha]/2$  and  $\rho_{\alpha'\uparrow(\downarrow)}(\mu) = \rho_{\alpha'}(\mu)[1 + (-)p_{\alpha'}]/2$ , where  $p_{\alpha(\alpha')}$  is the spin polarization of the conductivity in the electrode. If spin-flip hopping at the contacts is forbidden, i.e.  $\lambda = 0$  in  $T$  and  $T'$ , and the magnetizations of the two electrodes are parallel to the quantization axis, we have

$$g(\mu, 0) \propto \sum_{ab} [(1 + p_\alpha p_{\alpha'}) (|\bar{G}_{ab}^r|^2 + |g_{ab}^r|^2 S_z^2) + 2(p_\alpha + p_{\alpha'}) \bar{G}_{ab}^r g_{ab}^a S_z + (p_\alpha - p_{\alpha'}) |g_{ab}^r|^2 (S_x^2 + S_y^2)]. \quad (10)$$

According to equation (10), the conductance  $g(\mu, 0)$  contains a linear term of  $S_z$  but only quadratic terms of  $S_x$  and  $S_y$ , indicating that the sign of  $S_z$  can be detected. The coefficient of those quadratic terms is much smaller than that of the

linear term, by a factor of  $|g_{ab}^r|/|\bar{G}_{ab}^r| \sim |J/\epsilon_m| \simeq 10^{-4}$  in the non-resonant tunneling regime. Thus this electrical detection is much more sensitive to the longitudinal spin component than the transverse one. Furthermore, that linear term is proportional to the total spin polarization of the two electrodes,  $p_\alpha + p_{\alpha'}$ , suggesting that ferromagnetic electrodes would greatly enhance the spin signals in electrical transport compared to nonmagnetic electrodes that are used in most EDSR experiments. This is readily seen because the spin polarization in a nonmagnetic electrode is estimated as  $p_\alpha = \tanh(g_e \mu_B H_0 / E_F)$ , where  $g_e$  is the electrode  $g$  factor,  $H_0$  the applied magnetic field,  $E_F$  the Fermi energy of the electrode and  $p_\alpha \simeq 10^{-6}$  in metallic and  $10^{-4}$  in semiconducting electrodes. In contrast,  $p_\alpha \simeq 0.5$  in a typical ferromagnetic electrode. Thus the ferromagnetic electrodes perform the function of providing spin-polarized conduction electrons to enhance the spin–spin coupling between the carriers and the local spin at the central N atom. Injection of spin-polarized carriers into nonmagnetic materials using ferromagnetic electrodes is an important topic in the emerging field of spintronics. In a typical spintronic structure, a DC magnetic field is used to change the relative orientation of the electrode magnetizations and to achieve a large static magnetoresistance. In the device structure discussed here, an AC magnetic field is used to excite the local spin and a dynamic electrical transport is measured, which can be viewed as a new kind of spintronic device [5].

To perform EDSR using magnetic electrodes, one needs to ensure that the microwave did not cause ferromagnetic resonance in the electrodes. This can be achieved by choosing magnetic electrodes with a very different  $g$  factor than that in the sample whose ESR is to be detected. If the spin-flip hopping is partially allowed, the conductance will contain an additional term  $g_{\text{sf}}(\mu, 0)$ , which, to the first order of  $\lambda$ , is

$$g_{\text{sf}}(\mu, 0) \propto \sum_{ab} [2g_{ab}^r \bar{G}_{ab}^a (\lambda_1 S_x - \lambda_2 S_y) + (p_\alpha + p_{\alpha'}) |g_{ab}^r|^2 (\lambda_1 S_x - \lambda_2 S_y) S_z]. \quad (11)$$

We see that the real ( $\lambda_1$ ) and imaginary ( $\lambda_2$ ) parts of the spin-flip hopping exposes the transverse components  $S_x$  and  $S_y$  to the electrical transport.

#### 4. Spin dynamics and its signatures in transport

Now we examine the manifestation of the dynamics of the central spin in the conductance. The spin dynamics, including resonance, precession and relaxation, can be described by the Bloch equation:

$$\frac{d\mathbf{S}}{dt} = \gamma \mathbf{S} \times \mathbf{H} - \frac{S_x \mathbf{e}_x + S_y \mathbf{e}_y}{T_2} - \frac{S_z - S_0}{T_1} \mathbf{e}_z. \quad (12)$$

The Bloch equation is valid for both an individual spin and an ensemble average of spins (magnetization). Here  $\gamma = g_N \mu_B / \hbar$  is the magnetogyric ratio with  $g_N$  being the  $g$  factor for the electron spin in N@C<sub>60</sub>, which is 2, identical to that for a free electron [1], and  $\mu_B$  the Bohr magneton.  $\mathbf{H}$  is the total applied magnetic field, consisting of a DC field  $\mathbf{H}_0$  along the  $z$  axis and a circularly polarized microwave field with a frequency

$\omega$  in the neighborhood of the resonance frequency  $\omega_0 = \gamma H_0$ ,  $\mathbf{H}_1 = H_1(e_x \cos \omega t + e_y \sin \omega t)$ .  $S_0$  is the equilibrium value of the spin, and  $T_1$  and  $T_2$  are the longitudinal and transverse spin relaxation times which, according to [1] and [4], are caused by  $C_{60}$  vibrations for an isolated N@C<sub>60</sub> molecule.

Equation (12) neglects spin relaxation due to spectral diffusion caused by flip-flops of nuclear spins since for N@C<sub>60</sub> the spectral diffusion from the N nuclear spin was found to be insignificant for electron spin relaxation compared to the two-phonon process [2] and there exist no other nuclear spins near the central N atom in the proposed device structure. However, in the presence of electron conduction, the fluctuating electrical current, which creates a varying magnetic field  $\delta H(t)$  at the N atom, may also contribute to spin relaxation. Such a contribution can be estimated as  $1/T_1' \sim g_N^2 \mu_B^2 \overline{(\delta H)^2} \tau_c / \hbar^2$  [19], where  $\tau_c$  is the correlation time of the current fluctuation. For a molecular junction, the current fluctuation is at most around the nA range and the resultant  $\overline{(\delta H)^2}$  is less than  $10^{-3}$  G<sup>2</sup> [20].  $\tau_c$  should be close to the lifetime of vibrational modes in C<sub>60</sub>, which is  $10^{-11}$ – $10^{-12}$  s [21]. We have  $1/T_1' \leq 0.1$ – $1$  Hz, which is orders of magnitude smaller than  $1/T_1$  for an isolated N@C<sub>60</sub>. Hence we can safely neglect possible spin relaxation caused by the electrical current, and the values of  $T_1$  and  $T_2$  obtained from this electrical detection can be regarded as the intrinsic values of an isolated N@C<sub>60</sub>.

The Bloch equation is analytically solvable and the general solution of  $\mathbf{S}$  can be written as  $q = (x, y, z)$  [22]:

$$S_q = C_1 e^{-\zeta \tau} + C_2 e^{-\xi \tau} \cos \eta \tau + \frac{C_3}{\eta} e^{-\xi \tau} \sin \eta \tau + C_4, \quad (13)$$

where  $\tau = \gamma H_1 t$  and the eigenvalues  $\zeta$  and  $\xi \pm i\eta$  are the three roots of the cubic equation,  $(x + \phi)(x + \eta)^2 + x + \eta + \kappa^2(x + \phi) = 0$ , where  $\phi = 1/\gamma H_1 T_1$ ,  $\eta = 1/\gamma H_1 T_2$  and  $\kappa = (\omega_0 - \omega)/\gamma H_0$ . The coefficients  $C_i$  ( $i = 1, \dots, 4$ ) are determined by the initial conditions and asymptotic behavior at  $t = \infty$ .

The Bloch equation has a steady-state solution, where  $S_x$  and  $S_y$  precess around  $\mathbf{H}_0$  at frequency  $\omega$  and  $S_z$  remains constant,  $\tilde{S}_x = \Delta\omega \gamma H_1 T_2^2 S_0 / [1 + (T_2 \Delta\omega)^2 + \gamma^2 H_1^2 T_1 T_2]$ ,  $\tilde{S}_y = \gamma H_1 T_2 S_0 / [1 + (T_2 \Delta\omega)^2 + \gamma^2 H_1^2 T_1 T_2]$  and

$$\tilde{S}_z = S_z = \frac{1 + (\Delta\omega T_2)^2}{1 + (T_2 \Delta\omega)^2 + \gamma^2 H_1^2 T_1 T_2} S_0, \quad (14)$$

where  $\tilde{S}_q$  is the spin component in a frame rotating around the  $z$  axis with frequency  $\omega$ . The deviation of  $S_z$  from its equilibrium value,  $S_0$ ,  $S_z - S_0 = -\gamma^2 H_1^2 T_1 T_2 S_0 / [1 + T_2 (\Delta\omega)^2 + \gamma^2 H_1^2 T_1 T_2]$ , has a minimum at the resonance,  $\Delta\omega = 0$  and a Lorentz profile with a half-width of  $T_2^{-1} (1 + \gamma^2 H_1^2 T_1 T_2)^{1/2}$ . Since the conductance is sensitive to  $S_z$ , we expect that the resonance can be detected in electrical transport by continuously changing  $\omega$ . In most EDESR experiments, the microwave frequency  $\omega$  is fixed and the DC magnetic field  $H_0$  is swept to meet the resonance condition. Figure 2 shows the calculated conductance change,  $\Delta g = g(\mu, 0) - g_0$ , with  $g_0$  being  $g(\mu, 0)$  in the absence of the microwave  $\mathbf{H}_1$ , as a function of  $\Delta H = \omega/\gamma - H_0$ .  $S_0$  is fixed at  $S_0 = 0.25$ .

We assumed in the calculation that the sweeping rate of the magnetic field is slow compared to the spin relaxation time so that no memory effect is present. The conductance reaches a maximum at the resonance and its dependence on  $\Delta H$  is a mirror image of that on  $S_z$ . The relative conductance change of  $\Delta g/g_0 \sim 10^{-4}$  is remarkable, for EDESR can routinely detect the relative current change of  $10^{-9}$ . The derivative plot,  $d\Delta g/dH$  versus  $H$ , also shown in figure 2, is widely used to pinpoint the magnetic field  $H_0$  at which the spin resonance occurs [ $(d\Delta g/dH)_{H_0} = 0$ ] and the material's  $g$  factor can be obtained from  $g_N = \omega/\mu_B H_0$ . We also compare the signals between ferromagnetic and nonmagnetic electrodes in figure 2. For a small  $p_\alpha = 10^{-4}$ , a typical value for nonmagnetic electrodes, the signals are four orders of magnitude smaller than those with  $p_\alpha = 0.5$ , a typical value for magnetic electrodes. We emphasize that the results displayed in figure 2 and in figures to be shown later remain valid for detecting a single spin except the signals would become more pronounced. For a single spin with  $S = 3/2$ ,  $|S_0| = 3/2$  or  $1/2$ , which is greater than the value used in the calculations,  $S_0 = 0.25$ .

Spin relaxation times  $T_1$  and  $T_2$  are important to characterize spin dynamics. From the steady-state signal discussed above, we see that the width of the  $\Delta g/g$  peaks is a function of  $T_1$ ,  $T_2$  and  $H_1$ . Hence by measuring the widths at different microwave strength  $H_1$ , as shown in figure 2, one can determine  $T_1$  and  $T_2$ . To detect spin dynamics in an ensemble of molecules, however, the width shown in the conductance change will be mainly determined by inhomogeneous broadening because individual spins may have a slightly different resonance frequency. This is why steady-state EDESR usually is inadequate in measuring  $T_1$  and  $T_2$ , although it is very sensitive in probing the resonance frequency. One way to overcome this difficulty is to use short microwave pulses and measure the transient response in conductance. For a spin in equilibrium at  $t = 0$ ,  $S_z(0) = S_0$  and  $S_x = S_y = 0$ . Transverse magnetization can be created by applying a rotating field  $H_1$  for a time  $t_0$ . If the frequency is equal to the Larmor frequency  $\omega_0$ , at the end of the pulse,  $S_z(\tau) = S_0 \cos \omega_1 t_0$  and  $S_+(\tau) \equiv S_x(t_0) + i S_y(t_0) = S_0 \sin \omega_1 \tau \exp(i\omega_0 \tau)$ , where  $\omega_1 = \gamma H_1$ . After a  $\pi$  pulse, i.e.  $\omega_1 t_0 = \pi$ ,  $S_z$  would change from  $S_0$  to  $-S_0$  and  $S_x$  and  $S_y$  remain zero. After a  $\pi/2$  pulse, i.e.  $\omega_1 \tau = \pi/2$ , the spin changes its orientation from the  $z$  axis to the  $x$  axis. To measure  $T_1$ , we can apply a  $\pi$  pulse at  $t = 0$  and then turn off  $H_1$  and monitor the conductance change. The dynamics of  $S_z$ , from the Bloch equation, is

$$S_z(t) = S_0(1 - 2e^{-t/T_1}), \quad (15)$$

and the conductance change is displayed in figure 3. We see that the conductance change exponentially decays over time with the lifetime of  $T_1$ . This time dependence in the conductance signal does not change even if spin-flip hopping is allowed, as shown in figure 3, for the transverse spin component remains zero in this process and there is no additional contribution to the conductance from equation (14).

To measure  $T_2$ , one may think to use a  $\pi/2$  pulse and observe the free precession of  $S_x$ , which decays at a rate of  $T_2^{-1}$ . However, according to the Bloch equation,  $S_z$  will gradually increase from zero,  $S_z(t) = S_0(1 - e^{-t/T_1})$ , and

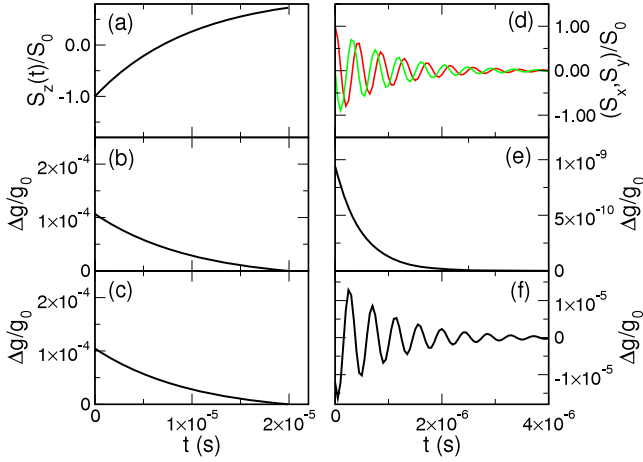


**Figure 3.** Transient relative conductance change due to longitudinal and transverse spin relaxation in N@C<sub>60</sub>. Panel (a) describes the free relaxation of  $S_z$  after a  $\pi$  pulse, and panels (b) and (c) plot the corresponding evolution of  $\Delta g/g_0$  with spin-flip hopping forbidden ( $\lambda = 0$ ) and spin-flip hopping allowed ( $\lambda_1 = \lambda_2 = 0.05$ ), respectively. Panel (d) describes the damped precession of transverse spin components,  $S_x$  (red or dark-gray line) and  $S_y$  (green or light-gray line) after a  $\pi/2$  pulse followed by an on-resonance microwave  $H_1 = H_1(\cos \omega_0 t e_x + \sin \omega_0 t e_y)$ . Panels (e) and (f) plot the corresponding  $\Delta g/g_0$  as a function of time with  $\lambda = 0$  and  $\lambda_1 = \lambda_2 = 0.05$ , respectively.  $T_1 = 10T_2 = 10^{-5}$  s. Other parameters are the same as in figure 2.

obscure the signal caused by the precession of  $S_x$ . One way to circumvent this occurrence is to follow a  $\pi/2$  pulse with a large  $H_1$  with the resonance frequency. Under this condition,

the asymptotic solution at  $t \rightarrow \infty$  is  $\tilde{S}_x(\infty) = \tilde{S}_y(\infty) = \tilde{S}_z(\infty) = 0$  and the initial condition is  $\tilde{S}_x = S_0$ ,  $\tilde{S}_y = S_z = 0$ . Thus we have  $S_+(t) = S_0 e^{-t/T_2} e^{-i\omega_0 t}$  and  $S_z(t) = 0$ . However, the conductance change in this scheme is weak, for the contribution from  $S_x$  and  $S_y$  is small compared with that from  $S_z$  as discussed earlier. When the spin-flip hopping is allowed, as mentioned earlier, the conductance would contain terms proportional to the transverse component and display a strong signal with a similar shape to  $S_x$ , as shown in figure 3. The oscillating signal in figure 3(f) indicates that the device conductance in the presence of spin dynamics can increase or decrease from the equilibrium value  $g_0$ .

An alternative and more appealing way to measure  $T_2$  is to use transient nutation, which employs a large  $H_1$  with  $\gamma H_1 \gg 1/T_2$ . Under this condition, the spin precesses around  $H_1$  in the rotating frame, which makes  $S_z$  subject to both longitudinal and transverse spin relaxation. The initial condition before the application of  $H_1$  is  $\tilde{S}_x = \tilde{S}_y = 0$  and  $S_z = S_0$ , at resonance ( $\kappa = 0$ ). From the general solution

$$S_z \simeq S_0 \exp\left[-\frac{1}{2}\left(\frac{1}{T_1} + \frac{1}{T_2}\right)t\right] \left(\cos \tau + \frac{\eta - \phi}{2} \sin \tau\right), \quad (16)$$

we see that  $S_z$  decays with a time constant  $2(T_1^{-1} + T_2^{-1})^{-1}$ , which is  $1/2T_2$  when  $T_2 \ll T_1$  and  $T_2$  if  $T_2 = T_1$ . Thus the transient nutation allows a sensitive measurement of  $T_2$  in the conductance change. We solve the Bloch equation for a different microwave frequency  $\omega$  and calculate the conductance change as a function of  $\omega$  and  $t$ , which is displayed in the color map of figure 4. We see that the

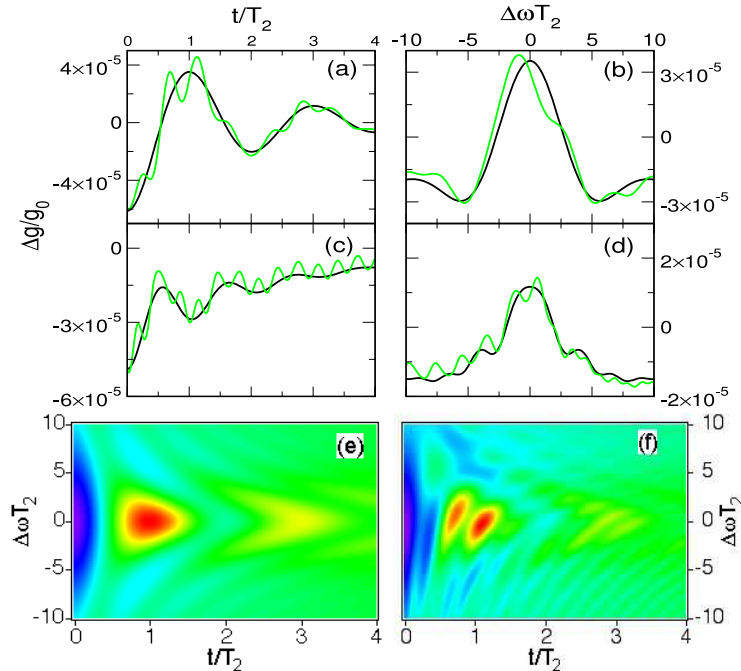


**Figure 4.** Conductance change spectrum due to transient nutation in the presence of a DC magnetic field  $H_0$  and a strong microwave  $H_1 = H_1(\cos \omega t e_x + \sin \omega t e_y)$ .  $\Delta g/g_0$  as a function of  $\Delta \omega \equiv \omega - \omega_0$  and  $t$  are plotted in a color or gray-scale map for  $\lambda = 0$  (e) and  $\lambda_1 = \lambda_2 = 0.05$  (f). Panels (a) and (b) describe  $\Delta g/g_0$  as a function of  $t/T_2$  for  $\Delta \omega T_2 = 0$  (on-resonance) and 5 (off-resonance), respectively. Panels (c) and (d) describe  $\Delta g/g_0$  as a function of  $\Delta \omega T_2$  for  $t/T_2 = 1$  and 3, respectively. Black lines are from panel (e) and green (gray) lines from panel (f).  $H_1 = 0.18$  G. Other parameters are the same as in figure 3.

change in conductance exhibits a damped oscillation. The oscillation is most pronounced near the resonance  $\Delta\omega T_2 \leq 1$  and becomes diminished when away from the resonance. The time constant for the envelope function both on- and off-resonance is comparable to  $T_2$ . This color map resembles that in measured EDESR in  $C_{60}$  [12], and its features survive when the spin-flip hopping is allowed, as shown in the figure. The small splitting in the conductance peak around  $\Delta\omega T_2 = 0$  can be used to estimate the relative importance of the spin-flip hopping.

## 5. Summary

In summary, we have developed a non-equilibrium Green's function formalism to describe how the dynamics of electron spin at the central N atom in  $N@C_{60}$  influences the electrical transport across the molecule when connected to magnetic electrodes. The  $\pi$ -conjugated  $C_{60}$  provides a highly conductive path for electron transport without blemishing the central spin and enables a noninvasive electrical detection of its dynamics. Steady-state spin resonance and transient spin motions can manifest themselves in the device conductance. We predict that magnetic electrodes can enhance the detectivity by orders of magnitude compared with nonmagnetic electrodes. The transient spin nutation is particularly useful for measuring  $T_2$  in this device structure because this electrical detection is more sensitive to the longitudinal spin component than the transverse one. This microscopic theory provides a framework to understand pulsed EDESR experiments in  $C_{60}$  and other similar systems.

## Acknowledgments

The author is grateful to M A Berding and S Krishnamurthy for helpful discussions. This work was supported by the Office of

Basic Energy Sciences, US Department of Energy, under grant no. DE-FG02-06ER46325.

## References

- [1] Morton J J L, Tyryshkin A M, Ardavan A, Porfyraakis K, Lyon S A and Briggs G A D 2006 *J. Chem. Phys.* **124** 014508
- [2] Morton J J L, Tyryshkin A M, Ardavan A, Porfyraakis K, Lyon S A and Briggs G A D 2007 *Phys. Rev. B* **76** 085418
- [3] Harneit W 2002 *Phys. Rev. A* **65** 032322
- [4] Yu Z G 2008 *Phys. Rev. B* **77** 205439
- [5] Awschalom D D, Loss D and Samarth N (ed) 2002 *Semiconductor Spintronics and Quantum Computation* (Berlin: Springer)
- [6] Honig A 1966 *Phys. Rev. Lett.* **17** 186
- [7] Elste F and Timm C 2005 *Phys. Rev. B* **71** 155403
- [8] Grose J E, Tam E, Timm C, Scheloske M, Ulgut B, Parks J J, Abruña H D, Harneit W and Ralph D C 2008 *Nat. Mater.* **7** 884
- [9] See, for example, Bolotov L, Uchida N and Kanayama T 2003 *J. Phys.: Condens. Matter* **15** S3065
- [10] König J and Martinek J 2003 *Phys. Rev. Lett.* **90** 166602
- [11] Abragam A 1961 *The Principles of Nuclear Magnetism* (London: Oxford) p 68
- [12] Harneit W, Boehme C, Schaefer S, Huebener K, Fostiropoulos K and Lips K 2007 *Phys. Rev. Lett.* **98** 216601
- [13] McCamey D R, Seipel H A, Paik S-Y, Walter M J, Borys N J, Lupton J M and Boehme C 2008 *Nat. Mater.* **7** 723
- [14] Joachim C and Gimzewski J K 1995 *Europhys. Lett.* **30** 409
- [15] Caroli C, Combescot R, Nozières P and Saint-James D 1971 *J. Phys. C: Solid State Phys.* **4** 916
- [16] Meir Y and Wingreen N S 1993 *Phys. Rev. Lett.* **68** 2512
- [17] Su W P, Schrieffer J R and Heeger A J 1980 *Phys. Rev. B* **22** 2099
- [18] Yu Z G, Sun X and Nasu K 1995 *Phys. Rev. B* **51** 7451
- [19] Slichter C P 1978 *Principles of Magnetic Resonance* (Berlin: Springer) p 181
- [20] Yu Z G 2008 *Phys. Rev. B* **78** 212411
- [21] Martin M C, Fabian J, Godard J, Bernier P, Lambert J M and Mihalý L 1995 *Phys. Rev. B* **51** 2844
- [22] Torrey H C 1949 *Phys. Rev.* **76** 1059